



## Original Article

# Microcephaly, intractable seizures and developmental delay caused by biallelic variants in *TBCD*: further delineation of a new chaperone-mediated tubulinopathy

Pode-Shakked B., Barash H., Ziv L., Gripp K.W., Flex E., Barel O., Carvalho K.S., Scavina M., Chillemi G., Niceta M., Eyal E., Kol N., Ben-Zeev B., Bar-Yosef O., Marek-Yagel D., Bertini E., Duker A.L., Anikster Y., Tartaglia M., Raas-Rothschild A. Microcephaly, intractable seizures and developmental delay caused by biallelic variants in *TBCD*: further delineation of a new chaperone-mediated tubulinopathy. Clin Genet 2017; 91: 725–738. © John Wiley & Sons A/S. Published by John Wiley & Sons Ltd, 2016

Microtubule dynamics play a crucial role in neuronal development and function, and several neurodevelopmental disorders have been linked to mutations in genes encoding tubulins and functionally related proteins. Most recently, variants in the tubulin cofactor D (*TBCD*) gene, which encodes one of the five co-chaperones required for assembly and disassembly of  $\alpha/\beta$ -tubulin heterodimer, were reported to underlie a recessive neurodevelopmental/neurodegenerative disorder. We report on five patients from three unrelated families, who presented with microcephaly, intellectual disability, intractable seizures, optic nerve pallor/atrophy, and cortical atrophy with delayed myelination and thinned corpus callosum on brain imaging. Exome sequencing allowed the identification of biallelic variants in *TBCD* segregating with the disease in the three families. *TBCD* protein level was significantly reduced in cultured fibroblasts from one patient, supporting defective *TBCD* function as the event underlying the disorder. Such reduced expression was associated with accelerated microtubule re-polymerization. Morpholino-mediated *TBCD* knockdown in zebrafish recapitulated several key pathological features of the human disease, and *TBCD* overexpression in the same model confirmed previous studies documenting an obligate dependency on proper *TBCD* levels during development. Our findings confirm the link between inactivating *TBCD* variants and this newly described chaperone-associated tubulinopathy, and provide insights into the phenotype of this disorder.

### Conflict of interest

The authors declare that they have no competing financial interests.

**B. Pode-Shakked**<sup>a,b,c,†</sup>,  
**H. Barash**<sup>a,†</sup>, **L. Ziv**<sup>d,†</sup>,  
**K.W. Gripp**<sup>e</sup>, **E. Flex**<sup>f</sup>, **O. Barel**<sup>d</sup>,  
**K.S. Carvalho**<sup>g</sup>, **M. Scavina**<sup>h</sup>,  
**G. Chillemi**<sup>i</sup>, **M. Niceta**<sup>j</sup>,  
**E. Eyal**<sup>d</sup>, **N. Kol**<sup>d</sup>,  
**B. Ben-Zeev**<sup>b,k</sup>,  
**O. Bar-Yosef**<sup>b,k</sup>,  
**D. Marek-Yagel**<sup>b,l</sup>, **E. Bertini**<sup>j</sup>,  
**A.L. Duker**<sup>e</sup>, **Y. Anikster**<sup>b,l</sup>,  
**M. Tartaglia**<sup>l,‡</sup> and  
**A. Raas-Rothschild**<sup>a,b,‡</sup>

<sup>a</sup>The Institute for Rare Diseases, The Danek Gertner Institute of Human Genetics, Sheba Medical Center, Tel-Hashomer, Israel, <sup>b</sup>Sackler Faculty of Medicine, Tel-Aviv University, Tel-Aviv, Israel, <sup>c</sup>The Dr Pinchas Borenstein Talpiot Medical Leadership Program, Sheba Medical Center, Tel-Hashomer, Israel, <sup>d</sup>Sheba Cancer Research Center, Sheba Medical Center, Tel-Hashomer, Israel, <sup>e</sup>Division of Medical Genetics, A.I. duPont Hospital for Children, Wilmington, DE, USA, <sup>f</sup>Department of Hematology, Oncology and Molecular Medicine, Istituto Superiore di Sanità, Rome, Italy, <sup>g</sup>Section of Pediatric Neurology, St. Christopher's Hospital for Children, Drexel University College of Medicine, Philadelphia, PA, USA, <sup>h</sup>Division of Pediatric Neurology, A.I. duPont Hospital for Children, Wilmington, DE, USA, <sup>i</sup>SCAI-Super Computing Applications and Innovation Department, CINECA, Rome, Italy, <sup>j</sup>Genetics and Rare Diseases Research Division, Ospedale Pediatrico Bambino Gesù, Rome, Italy, <sup>k</sup>Pediatric Neurology Unit, Edmond and Lily Safra Children's Hospital, and <sup>l</sup>Metabolic Disease Unit, Edmond and Lily Safra Children's Hospital, Sheba Medical Center, Tel-Hashomer, Israel

†These authors contributed equally to the manuscript.

‡These authors contributed equally as the senior investigators in this project.

Key words: developmental delay – intractable epilepsy – microcephaly – TBCD – tubulin

Corresponding authors: Annick Raas-Rothschild, MD, The Institute for Rare Diseases, The Danek Gertner Institute of Human Genetics, Sheba Medical Center, Tel-Hashomer, Israel.

Tel.: +972 35303952;

fax: +972 35307725;

e-mail:

Annick.Rothschild@sheba.health.gov.il and

Marco Tartaglia, PhD, Genetics Rare Diseases Research Division, Ospedale Pediatrico Bambino Gesù, Viale di San Paolo, 15, 00146 Rome, Italy.

Tel.: +39 06 68593742;

fax: +39 06 68592904;

e-mail: marco.tartaglia@opbg.net

Received 5 September 2016, revised and accepted for publication 28 October 2016

The normal development and proper function of neurons require microtubules, which are dynamic polarized cytoskeletal structures participating in a wide variety of cellular functions including proliferation, migration, cell morphology and polarity, and intracellular trafficking (1). Microtubules are assembled from heterodimers of  $\alpha$ - and  $\beta$ -tubulin, which constitute a family of structurally related proteins that are expressed with a specific spatial and temporal expression pattern in post-mitotic neurons during cortical development (2). The assembly and disassembly of the  $\alpha/\beta$ -tubulin heterodimers control microtubule dynamics, and are dependent on several chaperone proteins, including cytosolic chaperonin, five additional co-chaperones termed tubulin cofactors A through E (TBCA–TBCE), and the ARL2 GTPase (3–7).

In the past few years, human cortical malformations and neurodevelopmental disorders have been linked to variants in genes encoding tubulins and microtubule-associated proteins (8–12). Altered microtubule function and dynamics have also documented to cause or contribute to neurodegenerative disorders (13–16). Most recently, Flex et al. (17) reported on the identification of biallelic variants in tubulin cofactor D (*TBCD*) in seven patients of five unrelated families as the cause of a previously unrecognized autosomal recessive encephalopathy characterized by intellectual disability, seizures, early onset cortical atrophy with hypomyelination, optic atrophy, thin corpus callosum, and progressive spasticity. At the same time, two other

groups independently reported on the identification of a similar neurodevelopmental/neurodegenerative condition due to biallelic variants in *TBCD* (18, 19). All three groups provided biochemical and functional evidence supporting the deleterious effects of the *TBCD* variants on *TBCD* expression/function, as well as on  $\alpha/\beta$ -tubulin heterodimer assembly and microtubule dynamics (17–19).

*TBCD* has been shown to be involved in microtubule assembly and disassembly, and is essential for spindle microtubule dynamics (5, 20–22). This chaperone plays a central role in the *de novo* assembly of the tubulin heterodimer. Specifically, it binds to  $\beta$ -tubulin, and constitutes a supercomplex with TBCE and  $\alpha$ -tubulin, which is a required step for  $\alpha/\beta$ -tubulin heterodimerization and polymerization of the heterodimers into microtubules. Disease-causing variants affect *TBCD* stability and function, and resulted in perturbed microtubule dynamics (17). Interestingly, *in vitro* and *in vivo* studies documented that both downregulation and overexpression of *TBCD* have deleterious effects on microtubule rearrangement and function (23–25).

Here, we report on five patients from three unrelated families exhibiting intellectual disability, absent speech, epilepsy, optic atrophy, microcephaly, and cortical atrophy due to biallelic variants in *TBCD*. We document reduced *TBCD* levels and perturbed microtubule dynamics in fibroblasts obtained from one subject, and provide evidence that *TBCD* silencing in zebrafish recapitulates major features observed in the human disease. The data

## Microcephaly, intractable seizures and developmental delay caused by biallelic variants in *TBCD*

reported here provide additional insights into the phenotype and natural history of this newly recognized tubulinopathy into the second decade of life, and the mutation spectrum of disease-causing *TBCD* variants.

### Patients and methods

#### Patients

Patients 1, 2, and 3 were evaluated at the Sheba Medical Center, Tel-Hashomer, Israel. Patients 4 and 5 were followed clinically at the A.I. duPont Hospital for Children, Wilmington, DE, and St. Christopher's Hospital for Children, Philadelphia, PA. In these sibs, genetic testing was performed on a clinical diagnostic basis. Written informed consent was obtained from the parents for genetic analysis. The study was approved by the respective Institutional Review Boards.

#### Clinical reports

**Family A.** Patient 1 is a 26 months old boy, first child born to non-consanguineous parents of Indian-Jewish (Cochin) descent. Family history was unremarkable. The patient first presented for genetic evaluation due to the combination of microcephaly, developmental delay, seizures, and hypotonia at age of 1 year (Table 1). He was born following an uneventful pregnancy, at 40 weeks of gestation, with a birth weight of ~2700 g and head circumference of 34 cm (20th centile). During infancy, he was followed in a neurosurgery clinic due to suspected craniosynostosis, which was later ruled out.

A brain magnetic resonance imaging (MRI) performed in infancy showed mild dilatation of the ventricles and subarachnoid spaces with diffuse thinning of the white matter and corpus callosum, evidence of mild secondary hypomyelination not involving the internal capsule, and normal cerebellum (Fig. 1). At 9 months, he was hospitalized due to a suspected febrile seizure. Lumbar puncture was performed and the results were normal. Electroencephalography (EEG) showed disorganized high amplitude delta wave background and multifocal polyspike discharges at moderate rate.

At the age of 2 years, the patient showed developmental delay, was non-verbal, and had stereotypic hand movements. He showed microcephaly (43 cm,  $-4$  SD), hypotonia, and right-sided plagiocephaly, low anterior hairline, large ears, pectus excavatum, right hand single transverse palmar crease and lateral deviation of the first toes. On neurological examination, he had normal cranial nerve function, central and peripheral hypotonia, hyporeflexia and reduced muscle power. He made good eye contact and followed objects, had primary reaching movements, and was able to roll and babble; however, he did not respond to his name. Overall, his developmental level is roughly equivalent to that of 6 months of age. Ophthalmologic evaluation at 2 years showed pallor of the optic disc, while visual evoked potentials (VEP) were normal.

Chromosomal deletions or duplications were ruled out using chromosomal microarray analysis (CMA). Chromosome X inactivation in DNA extracted from

maternal leukocytes showed random X inactivation (61:39). Metabolic screening included urine organic acid profile, serum ammonia and acylcarnitine levels, which were all within normal limits. Serum amino acid profile had shown high glutamine (1136 nmol/ml, normal range: 333–809) and proline levels (418 nmol/ml, normal range: 40–332). However, on a repeated test a normal profile was noted. Urine amino acid profile showed slightly high alanine levels (150  $\mu$ mol/mmol creatinine, normal range: 41–130) and was otherwise non-contributory. As the combination of signs and symptoms were not fully compatible with any specific known nosologic entity and the initial evaluation did not yield a diagnosis, whole-exome sequencing (WES) was performed, using a trio-based strategy.

**Family B.** Two sisters (patients 2 and 3) born to healthy consanguineous parents (first degree cousins) of Egyptian-Jewish descent, were followed in the Pediatric Neurology Unit from infancy to the second decade of life, due to a combination of severe epilepsy, microcephaly, aphasia, intellectual disability and severe behavioral disorder (Table 1).

#### Patient 2

Currently 19 years old, the elder of the two siblings was reported to have had a normal neonatal course and achieve appropriate developmental milestones (including cruising, communicating, vocabulary of two words and a normal play pattern) until 11 months of age. Head circumference was 43.9 cm at 15 months (15th centile). During the second year of life, slowing of development was noticed accompanied by frequent focal clonic and generalized tonic clonic seizures (GTC's), partially related to febrile illnesses, and very frequent atypical absence seizures. Over almost two decades of follow up, seizures were intractable and refractory to numerous anticonvulsants, ketogenic diet and Cannabidiol enriched cannabis. She gained independent walking at age 3 years with an ataxic-spastic gait. She had severe cognitive disability, did not develop verbal abilities, and had consistent behavioral problems characterized by aggressiveness, restlessness and severe sleep disturbance only partially responsive to medication. There was no evidence for neurological deterioration after the first 2 years. At age of 19 years, circumference was 49 cm,  $-4$  SD.

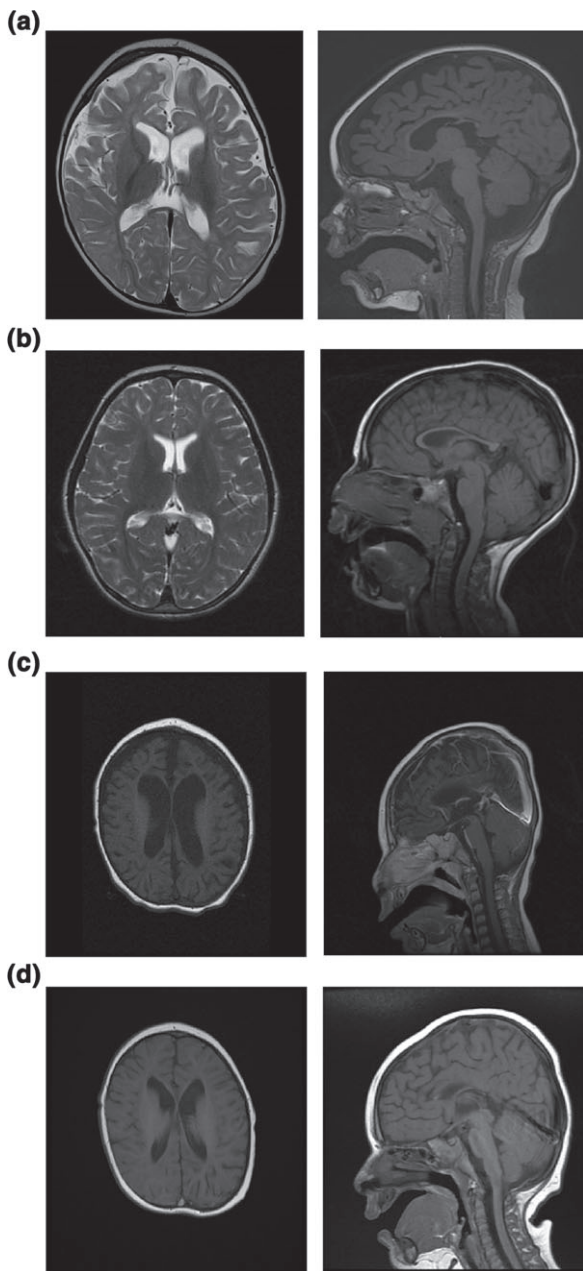
An extensive diagnostic evaluation ensued. Repeated EEG showed frequent generalized polyspike and wave discharges with intermittent slowing. Nerve conduction studies, electromyography (EMG) and VEP (performed at 17 months) were all considered normal. At 6 years, MRI showed mild cortical atrophy and moderately thin corpus callosum, with no evidence for brain malformation or signal changes (Fig. 1). Metabolic workup, consisting of blood lactate, pyruvate, amino acid profile, uric acid, ammonia, cholesterol, carnitine and acyl carnitines, homocysteine, very long chain fatty acids (VLCFA), urine tests for organic acid profile, purines, guanidinoacetate and creatine, and cerebrospinal fluid (CSF) tests (lactate, glucose and amino acid profile) was

Table 1. Demographic, clinical and molecular data of patients with variants in *TBCD*

1	2 <sup>a</sup>	3 <sup>a</sup>	4	5	Flex et al. (17)	Edvardson et al. (18)	Miyake et al. (19)
Gender	M	F	M	M	3M, 4F	4F	3M, 5F
Ethnic background	Indian-Jewish (Cochin)	Egyptian-Jewish	German/Sicilian/ Cajun-Hungarian/ Irish	German/Sicilian/ Cajun-Hungarian/ Irish	Diverse	Indian-Jewish (Cochin); Palestinian-Muslim	Japanese; Chinese; Sephardic-Jewish
Consanguinity	No	Yes	No	No	No	Yes	1/4 families
Age at presentation	9 months	3 years	4.5 months	5 months	Infancy-early childhood	3–14 months	Birth to 11 months
Current age	2 years and 2 months	19 years	7 years	15 months	1–20 years	2–6 years	2–19 years
Microcephaly	+	+	+	+	4/7	4/4	8/8
Epilepsy	+	+	+	+	6/7	4/4	6/8
Intellectual disability	+	+	+	+	7/7	4/4	8/8
Optic atrophy	+	N/A	+	+	6/6	N/A	4/8
Hypotonia	+	–	–	–	5/7	–	6/8
Spasticity	–	+	+	+	7/7	2/4	N/A
Feeding difficulties	–	N/A	GERD, G-tube	G-tube	5/7	N/A	N/A
Skeletal involvement	Plagiocephaly, pectus excavatum	N/A	–	Plagiocephaly	Plagiocephaly (1/7), pectus scoliosis (6/7), pectus carinatum (1/7)	N/A	N/A
Additional findings	Large ears, lateral deviation of first toes, stereotypic hand movements	Mild ataxia	EMG (3 years): severe motor axonal neuropathy; recurrent pneumonia (tracheostomy)	Short stature, neurogenic bladder, several tendon lengthening orthopedic surgeries	Diverse	DDH; dystonia; hirsutism; Strabismus; nystagmus (2/4)	Diverse
Brain MRI/MRA findings	Mild dilatation of the ventricles and subarachnoid spaces with suspected diffuse thinning of the white matter including corpus callosum	Mild cortical atrophy and moderately thin corpus callosum	Diffuse cerebral atrophy with thinning of corpus callosum	Diffuse white matter volume loss; partial agenesis of corpus callosum	Cortical atrophy, thin corpus callosum, cerebellum atrophy	Generalized brain atrophy, mainly of white matter, thin corpus callosum	Progressive enlargement of bilateral ventricles, thin corpus callosum, cerebellar atrophy
Variant(s) in <i>TBCD</i>	c.1423G>A (p.A475T)	c.2810C>G (p.P937R)	c.1757C>T (p.A586V); c.3192-2A>G (IVS34-2A>G)	c.1757C>T (p.A586V); c.3192-2A>G (IVS34-2A>G)	c.3365C>T (p.P1122L); c.3313G>A (p.V1105M); c.2981C>T (p.T994M); c.1130G>A (p.R377Q); c.1876G>A (A626T); c.771+1-771+10del; c.1121C>T (p.T374M); c.686T>G (p.L229R)	c.1423G>A (p.A475T); c.1757C>T (p.A586V)	c.1160T>G (p.M887R); c.1564-12C>G (p.G522Ffs*14); c.2208C>A (p.Y760*); c.2314C>T (p.R772C); c.2761G>A (p.R921T); c.2810C>G (p.P937R); c.3365C>T (p.Pro1122L)

+, present; –, absent; DDH, developmental dislocation of the hip; EMG, electromyography; F, female; GERD, gastroesophageal reflux disease; M, male; MRI, magnetic resonance imaging; MRA, magnetic resonance angiography; N/A, not available; TBCD, tubulin cofactor D.

<sup>a</sup>Note that patients 2 and 3 have also been reported as patients 7 and 8, respectively, by Miyake et al. (19).



**Fig. 1.** Brain magnetic resonance imaging (MRI) of patients with biallelic tubulin cofactor D (*TBCD*) variants. **(a)** Axial T2 MRI image of patient 1 (18 months), showing cortical atrophy and hypomyelination (with no involvement of the internal capsule (left)). Myelination age is equal to chronological age of 3–6 months. Sagittal T1 MRI image of patient 1 (18 months), showing cortical atrophy and thinning of corpus callosum with normal cerebellar and brain stem structure (right). **(b)** Axial (left) and sagittal (right) T1 MRI of patient 2 (6 years) showing mild cortical atrophy and moderately thin corpus callosum. **(c)** Axial (left) and sagittal (right) T1 MRI images of patient 4 (4 months) showing diffuse deficiency of the white matter in both cerebral hemispheres. Thinning of the corpus, as well as *ex vacuo* dilatation of lateral and third ventricles and mild enlargement of the extra axial fluid spaces, are probably attributable to the overall white matter deficiency. Pattern of myelination is appropriate for the patient's age. **(d)** Axial (left) and sagittal (right) T1 MRI images of patient 5 (6 months), indicating dilated supratentorial ventricular system with an irregular contour suggesting central greater than cortical volume loss. The corpus callosum is present but markedly thinned.

unremarkable. Finally, genetic workup included karyotype, fluorescence *in situ* hybridization and methylation studies for Angelman syndrome, CMA and sequencing of *MECP2*, *FOXP1* and *CDKL5*. All analyses reported normal results.

#### Patient 3

Currently 17 years old, patient 3 is the younger sister of patient 2. She was born following uneventful pregnancy and delivery, with no available information on head circumference at birth; however, the parents did report deceleration of head growth during the first year of life, and at 2.5 years her head circumference was 45.5 cm ( $-2$  SD). Patient 3 walked at 22 months, but did not develop speech. Seizures began at around 2 years and included occasional GTC's partially related to febrile illnesses, and very frequent atypical absence seizures. Developmental and behavioral features were similar to her older sister with severe cognitive disability, aphasia and severe behavioral problems, as well as mild ataxia and spasticity (Table 1). Similar to her sister, seizures proved to be intractable to multiple anticonvulsants.

With the clinical assumption that the two sisters probably suffered from the same inherited disorder, WES was pursued for the siblings and their parents.

**Family C.** Two brothers (patients 4 and 5), the only two children born to healthy non-consanguineous parents of German/Sicilian/Cajun-Hungarian/Irish descent, were followed by the Pediatric neurology team due to a combination of severe developmental delay, microcephaly and epilepsy refractory to treatment (Table 1).

#### Patient 4

Currently 7 years old, patient 4 was born at term to a 26 years old mother with prenatal care and no prenatal complications. He was born via spontaneous vaginal delivery, birth weight: 3540 g (60th centile), length: 53.3 cm (75th centile). Occipito-frontal circumference (OFC) at 9 days and 2 months reported to be in the 25th centile. He was reported to have some latching difficulties during the first few months, and gastroesophageal reflux disease, which spontaneously resolved. At 4.5 months, he was admitted to the hospital for status epilepticus. Sepsis work up was normal. At that time, he was noted to be microcephalic, weak, hypertonic and minimally interactive. He developed intractable epilepsy, and a vagal nerve stimulator was placed at 1 year after failing multiple antiepileptic medications. He was never able to roll, sit, crawl, walk or speak. Due to progressive feeding dysfunction a G-tube was placed at 4 years. He had recurrent admissions for pneumonias and respiratory distress and eventually underwent tracheostomy. At age 7 years, he had a head circumference of 43.9 cm ( $-4.5$  SD), weight was 21 kg (10th–25th centile). Height measurements were difficult to obtain, but consistently showed short stature with  $Z = -3$ . Physical examination was notable for right posterior plagiocephaly, otherwise he showed no clear dysmorphic features nor scoliosis.

He was ventilator-dependent with progressively increasing respiratory support needs. He had progressive weakness; an EMG performed at 3 years showed severe axonal motor neuropathy. Muscle biopsy showed neurogenic muscle atrophy. He was wheelchair-bound and immobile, and considered to have spastic quadriplegia. Ophthalmological examination showed optic nerve atrophy.

An extensive diagnostic investigation ensued. Brain MRI performed twice at 4 months showed diffuse cerebral atrophy, and at 3 years showed progressive gray and white matter atrophy. Spine MRI was considered normal at 4 years. CSF levels for neurotransmitter profile, lactate, pyruvate and amino acids were within normal limits, as were serum lactate, pyruvate, amino acids, carnitine and acylcarnitine, Creatine Kinase (CK), VLCFA, biotinidase, ammonia and transferrin electrophoresis studies. Urine oligosaccharides, organic acids and mucopolysaccharides were also considered normal. CMA showed a 6q16.3 deletion (100088936-100198541) (Hg18;2006), noted to be an equivocal result (parents not evaluated).

#### Patient 5

Currently 15 months old, he was born full term via spontaneous vaginal delivery, birth weight 3540 g, length 50.8 cm, with neither prenatal nor perinatal complications. Early development was considered normal, and he reportedly rolled over at 4 months and sat unassisted at 5 months. However, at 5 months he began experiencing seizures, which proved refractory to multiple antiepileptic medications. Before seizures onset he was able to reach, coo, follow and fix, smile and laugh. At 8 months, he was noted to have microcephaly (42 cm, -2.3 SD) and hypertonia. Vagal nerve stimulator was implanted at 9 months to assist with seizures control. At age 15 months he was unable to roll, sit, reach, track or laugh and had minimal social interaction. Physical examination showed no dysmorphic features nor scoliosis. He was non-communicative, had increased muscle tone in upper extremities and decreased tone in lower extremities, and lacked head control or purposeful hand movements. Brain MRI at 7 months showed partial agenesis of corpus callosum and diffuse cerebral atrophy. Ophthalmological evaluation showed bilateral optic nerve pallor. Finally, clinical WES was pursued for the siblings and their parents.

#### Methods

##### Whole-exome sequencing

After obtaining written informed consent from the parents, genomic DNA was extracted from peripheral blood leukocytes by standard procedures. Sequencing and data analysis methods are detailed in Appendix S1, Supporting information.

##### Structural analysis

Methods are detailed in Appendix S1.

##### Cell cultures

Methods are detailed in Appendix S1.

##### TBCD expression and microtubule re-polymerization studies

Methods are detailed in Appendix S1.

##### Zebrafish TBCD knockdown and rescue experiments

Methods are detailed in Appendix S1.

## Results

Three unrelated families were included in this study. Demographic, clinical and molecular data of the patients are summarized in Table 1.

#### WES results

Family A – WES data analysis yielded 11 homozygous private/rare variants affecting protein-coding sequences and transcript processing (Table S1). Among these, the c.1423G>A missense change in *TBCD* (NM\_005993.4), predicting the p.Ala475Thr amino acid substitution (NP\_005984.3), for which the proband was found to be homozygous and both parents heterozygous carriers (Fig. 2a), was considered as the most promising candidate. The variant had previously been annotated in ExAC (2/118538, heterozygous state), and was not found in our in-house WES databases nor in 80 alleles from Indian-Jewish (Cochin) unaffected individuals, using *Hinp*1I restriction enzyme analysis. The amino acid substitution was predicted to be damaging by different *in silico* tools (Polyphen2, LRT, variant Taster, FATHMM, Variant Assessor) (Polyphen2: <http://genetics.bwh.harvard.edu/pph2/>, Database of genomic variants: <http://projects.tcag.ca/variation/>, 1000 genome project: <http://www.1000genomes.org/>, SNAP: <http://roslab.org/services/snap/>). Consistently, the amino acid residue was found to be conserved throughout evolution (Fig. 2b). Of note, the c.1423G>A change was recently reported as the causative event underlying a similar clinical phenotype observed in two sisters born to an unrelated family of Indian-Jewish (Cochin) descent (18).

Family B – Based on the presence of two affected female siblings and parental consanguinity, autosomal recessive inheritance was hypothesized. WES data analysis yielded 10 homozygous rare variants predicted to have functional impact on coding sequences. Of these, the c.2810C>G (p.Pro937Arg) variant in *TBCD* was prioritized as the best candidate underlying the disorder. Genotyping of parental DNAs confirmed segregation (Fig. 2a). This variant had not been previously reported in public databases and had not been identified in our databases. The amino acid substitution affected a conserved residue (Fig. 2b) and was predicted to be damaging by different *in silico* tools (Polyphen2, LRT, Mutation Taster, Mutation Assessor).

Consistent with the causative role of each *TBCD* variant, no other gene with high-quality, functionally relevant



## Pode-Shakked et al.

biallelic changes was identified as candidate underlying the disease in the two families, and none of the genes with putative *de novo* variants were functionally linked to processes relevant to neurodevelopment and/or neurodegeneration. Moreover, sharing of the same candidate gene and the overlapping phenotype among patients strongly suggested that the biallelic variants in *TBCD* were causal.

**Family C** – In parallel, a third family with two affected siblings with similar clinical features was ascertained using clinical WES. WES data analysis revealed two different variants in the *TBCD* gene, c.1757C>T (p.Ala586Val) and c.3192-2A>G (IVS34-2A>G), for which the siblings were compound heterozygous and each parent carried one variant. These variants had not been previously reported in public databases. The p.Ala586Val affects a highly conserved residue, and is predicted to be damaging by multiple *in silico* tools. Similarly, the splice site change affects a canonical splice acceptor site in intron 34, and is predicted to cause aberrant transcript processing. Of note, the c.1757C>T variant has been reported in two sisters of Palestinian-Muslim descent with similar phenotype (18).

### Structural analysis

The affected residues mapped at different regions of the modeled structure of native *TBCD* obtained by homology modeling and validated by molecular dynamics (MD) simulation (Fig. 3a). Substitution of the hydrophobic residues Ala<sup>475</sup> and Pro<sup>937</sup> with threonine and arginine, respectively, were expected to strongly perturb the local structure of *TBCD* due to the different chemical-physical characteristics of the affected residues. Specifically, Pro<sup>937</sup> is part of a hydrophobic core stabilizing the relative position of two helices, which is predicted to be disrupted by the introduced positively charged residue (Fig. 3b). Similarly, Ala<sup>475</sup> is located in a buried and hydrophobic region, which contributes to the stability of the relative orientation of four helices (Fig. 3c), and the Ala-to-Thr substitution is expected to rearrange such structural organization.

In the modeled *TBCD* structure, Ala<sup>586</sup> is relatively close to Ala<sup>475</sup>. The p.Ala586Val change is conservative, with only a slight increase in steric volume. MD simulations performed to investigate the structural perturbation induced by the Ala-to-Val substitution documented that the introduction of the valine residue causes a local rearrangement of the structure by perturbing the interactions of helix 578–592 with adjacent helices (Fig. 3d). While all substitutions were predicted to have relevant structural impact, their long-range effects deserve further investigations.

### Impact on *TBCD* protein levels and microtubule dynamics

The recessive inheritance pattern suggested a loss-of-function mechanism exerted by the disease-associated *TBCD* variants. To explore a possible impact of the identified variants on protein

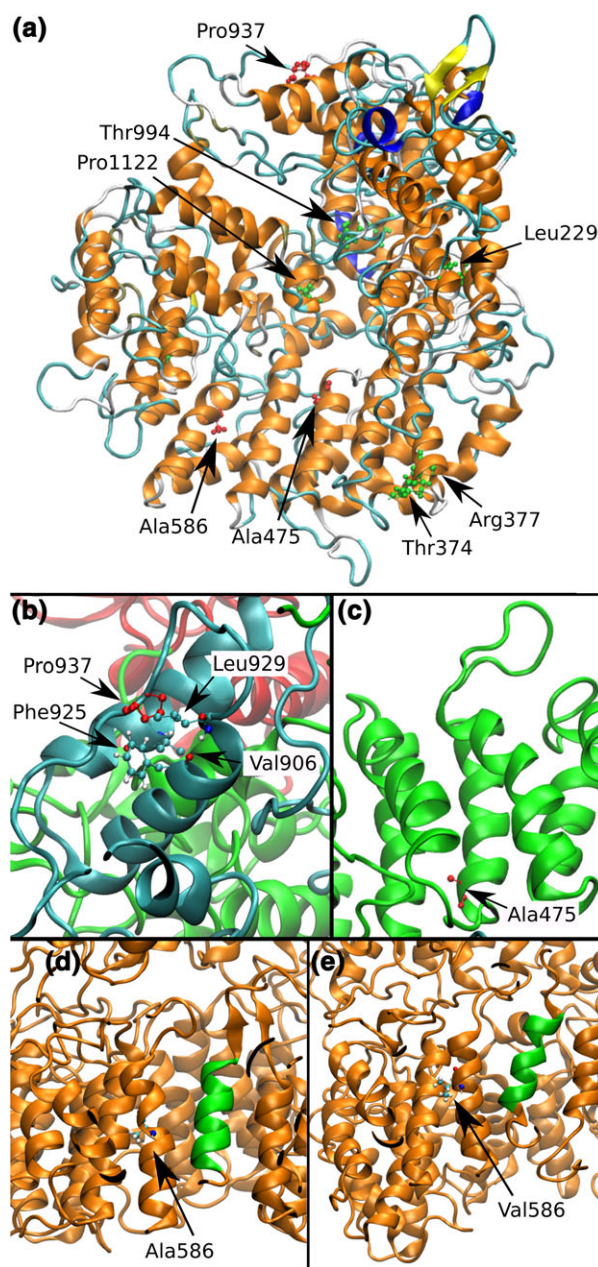


**Fig. 3.** Structural impact of the identified tubulin cofactor D (*TBCD*) variants. (a) Location of the three residues affected by the disease-associated amino acid substitutions (p.Ala475Thr, p.Ala586Val and p.Pro937Arg) (lateral chain highlighted in pink) in the *TBCD* structure (orange,  $\alpha$ -helix; yellow,  $\beta$ -strand; blue,  $3_{10}$  helix; cyan, turn). The location of residues previously reported to be affected in subjects with biallelic *TBCD* mutations is also shown (lateral chain highlighted in green). (b) Pro<sup>937</sup> with surrounding hydrophobic residues contribute to a hydrophobic core with a role in stabilizing the structure of protein locally. Residues participating in such interactions (distance < 3.6 Å) are indicated with their lateral chains. (c) Ala<sup>475</sup> is located in a buried and hydrophobic region, which contributes to the relative orientation of four  $\alpha$  helices in antiparallel conformation. (d) Ala<sup>586</sup> is a buried residue located in a region of  $\alpha$  helices. (e) MD simulations performed to investigate the structural perturbation induced by the Ala586Val substitution documented a local rearrangement of the structure affecting the interactions of these helices and resulting in a substantial rearrangement of their relative orientation. Color figure is available in Online version.

## Microcephaly, intractable seizures and developmental delay caused by biallelic variants in *TBCD*

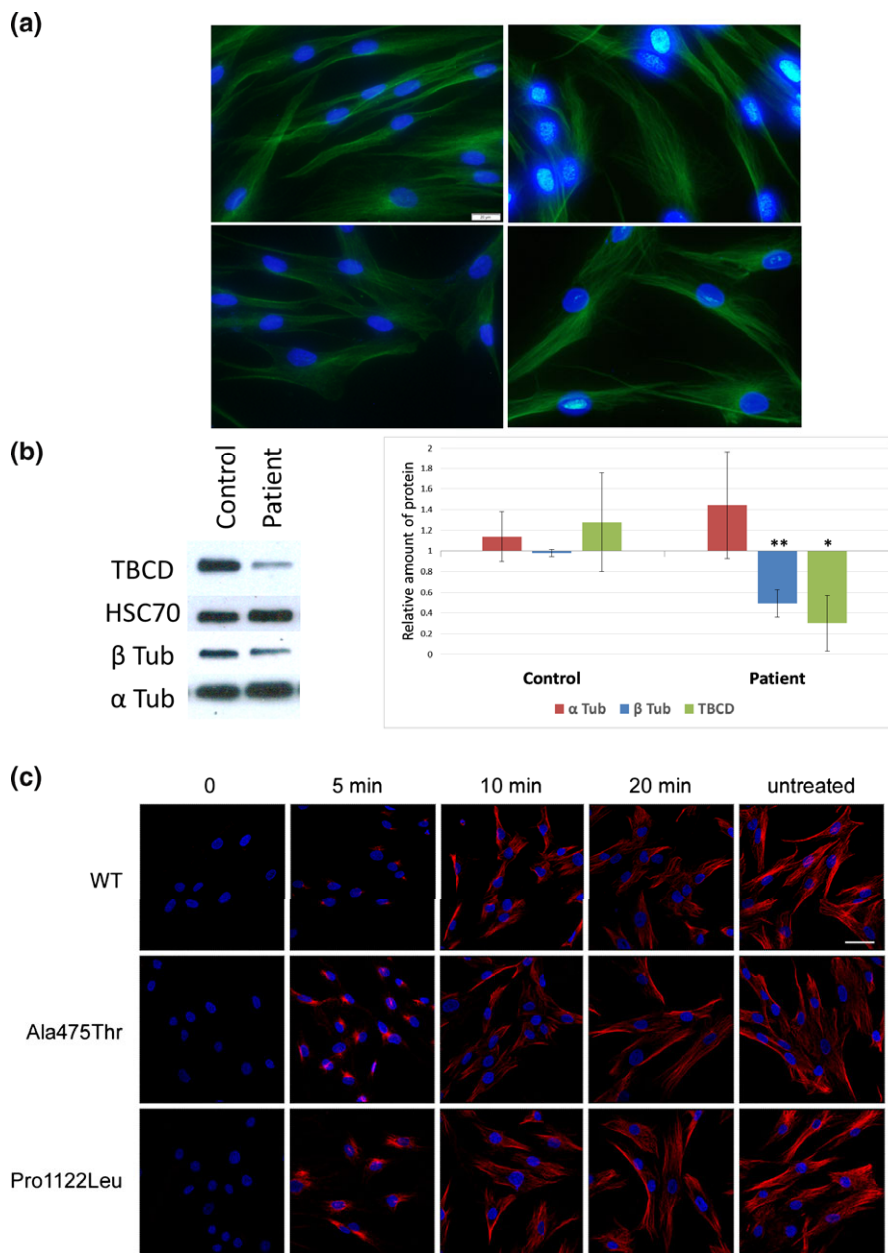


**Fig. 4.** Impact of the homozygous c.1423G>A missense change (p.Ala475Thr) in tubulin cofactor D (*TBCD*) on  $\beta$ -tubulin levels and microtubule dynamics. **(a)** Immunofluorescence analysis of cultured skin fibroblasts (patient 1) showing the reduced  $\beta$ -tubulin levels (left, bottom) compared with an unaffected age-matched individual (left, top). In contrast, no significant difference in the levels of  $\alpha$ -tubulin was documented between fibroblasts of the patient (right, bottom) and control (right, top). Scale bar (20  $\mu$ m) is the same for all panels. **(b)** Western blots from patient 1 immortalized B lymphocytes lysates showing reduced levels of TBCD and  $\beta$ -tubulin compared with control cells (left). Consistent with the immunofluorescence findings, no significant difference in the level of  $\alpha$ -tubulin was documented. HSC70 is shown as loading control. Densitometry of the western blots comparing the amount of protein in patient cells compared with control cells ( $n = 3$ ) is also shown (right). Results are displayed as average ( $\pm$ SD). \* $p < 0.05$ , \*\* $p < 0.01$ . **(c)** Accelerated microtubule re-polymerization. Representative confocal microscopy analysis of fibroblasts from patient 1 after nocodazole treatment and medium recovery showing accelerated microtubule re-polymerization compared with control cells. Such perturbed dynamics is less evident compared to what is observed in fibroblasts from a patient homozygous for the p.Pro1122Leu change, which dramatically affects protein stability and results in rapid degradation of the chaperone. Fixed cells were stained with anti- $\alpha$ -tubulin antibody (red) and DAPI (blue). Scale bar (47  $\mu$ m) is the same for all panels.  
Color figure is available in Online version.

synthesis/stability, qPCR and western blot assays were performed. No differences in the level of *TBCD* mRNA were detected between skin fibroblasts and lymphoblastoid lines obtained from patient 1 and two control individuals (data not shown). Western blot analysis

of protein lysate extracted from both immortalized B lymphocytes and fibroblasts; however, consistently documented a significant reduction in the amount of TBCD protein (Fig. 4a). Similar to what previously documented by Flex et al. (17) western blot and immunofluorescence

analyses did not outline any significant difference in the level of  $\alpha$ -tubulin between patient and control cell lines; however, a significant reduction in  $\beta$ -tubulin was documented (Fig. 4b), suggesting a possible impact of substantially reduced TBCD expression/function on  $\beta$ -tubulin availability in cells.

As defective TBCD function has been documented to affect microtubule dynamics (17), the kinetics of tubulin re-polymerization was assessed in primary fibroblasts from patient 1 and compared with controls and fibroblasts from a patient with severely impaired TBCD function (Fig. 4c). Following complete microtubule de-polymerization, recovery was allowed for 5, 10, and 20 min. Compared to what was observed in treated control fibroblasts, microtubule re-polymerization appeared to be accelerated in cells from patient 1, which is consistent with these mutations being hypomorphic (17). Of note, such perturbed dynamics was less marked compared with what was observed in fibroblasts with extremely reduced TBCD levels, which is in line with the overall less severe phenotype characterizing the present patient (17).

Phenotype analysis of morpholino-mediated TBCD silencing in zebrafish

Zebrafish *tbcd* protein shows 65% identity with human TBCD. *tbcd* morpholino (mo) was injected to zebrafish embryos at one cell stage, at different doses (0.12–0.2 mM). *tbcd* was significantly diminished in 0.14 mM injected larvae, and completely absent following 0.2 mM mo injection. *tbcd* knockdown (KD) animals presented with a phenotype that appeared from day 2. Major features in morphants included microcephalus, and small eyes (Fig. 5a,b). Other features also included short and thick tail, heart edema, and scattered pigment. A progressively more severe phenotype was observed at increasing mo dose, from 0.12 to 0.2 mM (Fig. 5a, from left to right). Overall, such phenotype was evident at the range of 80–85% (82.5% on average) of a total of 100 injected larvae analyzed in the three experiments with 0.2 mM mo. Histological analysis of morphants performed at 3 dpf revealed brain atrophy, with thin neural layers, decreased neural density and hydrocephalus (Fig. 5c,i). *tbcd*<sup>ATG</sup> mo presented reduced eye size (45%) with a defective lamination with absence of the nuclear and plexiform layers, in comparison to control larvae which displayed normal retinal lamination (Fig. 5c,ii). Finally, histology of muscle tissue of morphants showed myocyte disorganization and irregular myoseptae (Fig. 5c,iii).

Western blot analysis documented loss of  $\beta$ -tubulin which was consistently associated with reduced/abolished *tbcd* expression, while a dose-dependent reduction of  $\alpha$ -tubulin levels was noticed compared with uninjected larvae (Fig. 6a).

To further verify the specificity of *tbcd* mo effect on the phenotype observed in zebrafish larvae, *TBCD* cDNA was co-injected with *tbcd* mo (0.2 mM). Phenotypic analysis of the morphants documented a partial rescue of the phenotype, with 40% of the co-injected

embryos ( $n = 60$ ) exhibiting no apparent malformation, supporting the specificity of the phenotype due to *tbcd* modulation. High TBCD expression in the malformed fish concurred with high  $\beta$ -tubulin expression, compared to non-rescued larvae (Fig. 6b). Furthermore, compared to the latter, normal-appearing co-injected larvae exhibited a  $\beta$ -tubulin expression level similar to that observed in uninjected animals. Remarkably, overexpression of TBCD had similar phenotypic effects in injected larvae as *tbcd* downmodulation (Fig. 6c), strongly suggesting the need for an exact TBCD dosage for normal developmental processes.

## Discussion

Microtubule dynamics play a key role in an array of neuronal cellular functions, and therefore it has been predicted and shown that variants in the tubulin gene family (i.e. *TUBA1A*, *TUBA4A*, *TUBA8*, *TUBB2B*, *TUBB3*, *TUBB4A*, and *TUBB5*), as well as in genes encoding functionally related proteins (*TBCE*, among others) cause both brain cortical anomalies and neurodevelopmental/neurodegenerative disorders (8, 11–16, 26).

TBCD, one of the five tubulin co-chaperones, is crucial for the proper assembly and disassembly of the microtubules. Highly expressed in brain and spinal cord during fetal development, TBCD functions not only as a tubulin co-chaperone mediating proper folding and heterodimer assembly of tubulins but is also crucial for recruitment of the  $\gamma$ -tubulin ring complex located in centrosomes, the microtubule-organizing centers (23). Previous studies have shown that TBCD expression levels require an extremely fine equilibrium, with both under and overexpression causing disruption of normal neuronal morphogenesis (25). Furthermore, TBCD interacts with additional key players in neuronal development, such as Down syndrome cell adhesion molecule (Dscam) and Strip (25, 27). In addition, loss of TBCD in *Drosophila* results in abnormal arborization of dendrites and axonal degeneration while its overexpression is also associated with microtubules' disruption and ectopic dendrite arborization (25). Therefore, it was expected that any variant altering the fine tuning of the TBCD level and/or function would prove detrimental to normal brain cortical development and neuronal function. Nonetheless, until only very recently, no human phenotype had clearly been attributed to defective or aberrant TBCD function.

Interestingly, in 2014, Poulton et al. pointed out a possible contributing role of *TBCD* on the severity of the phenotype of a patient with severe microcephaly associated with a *WDR62* variant, and a missense change (p.Phe1121Val) and a duplication encompassing the wild type *TBCD* allele (28). Immunostaining showed an abnormal tubulin network in cells from the patient with both *WDR62* and *TBCD* variants. Very recently, a new disorder was linked to impaired TBCD function by three groups: Flex et al. (17) reported on seven individuals from five unrelated families exhibiting a previously unrecognized autosomal recessive trait characterized by neurodevelopmental and neurodegenerative features due to biallelic variants in *TBCD*. They documented that

## Microcephaly, intractable seizures and developmental delay caused by biallelic variants in *TBCD*

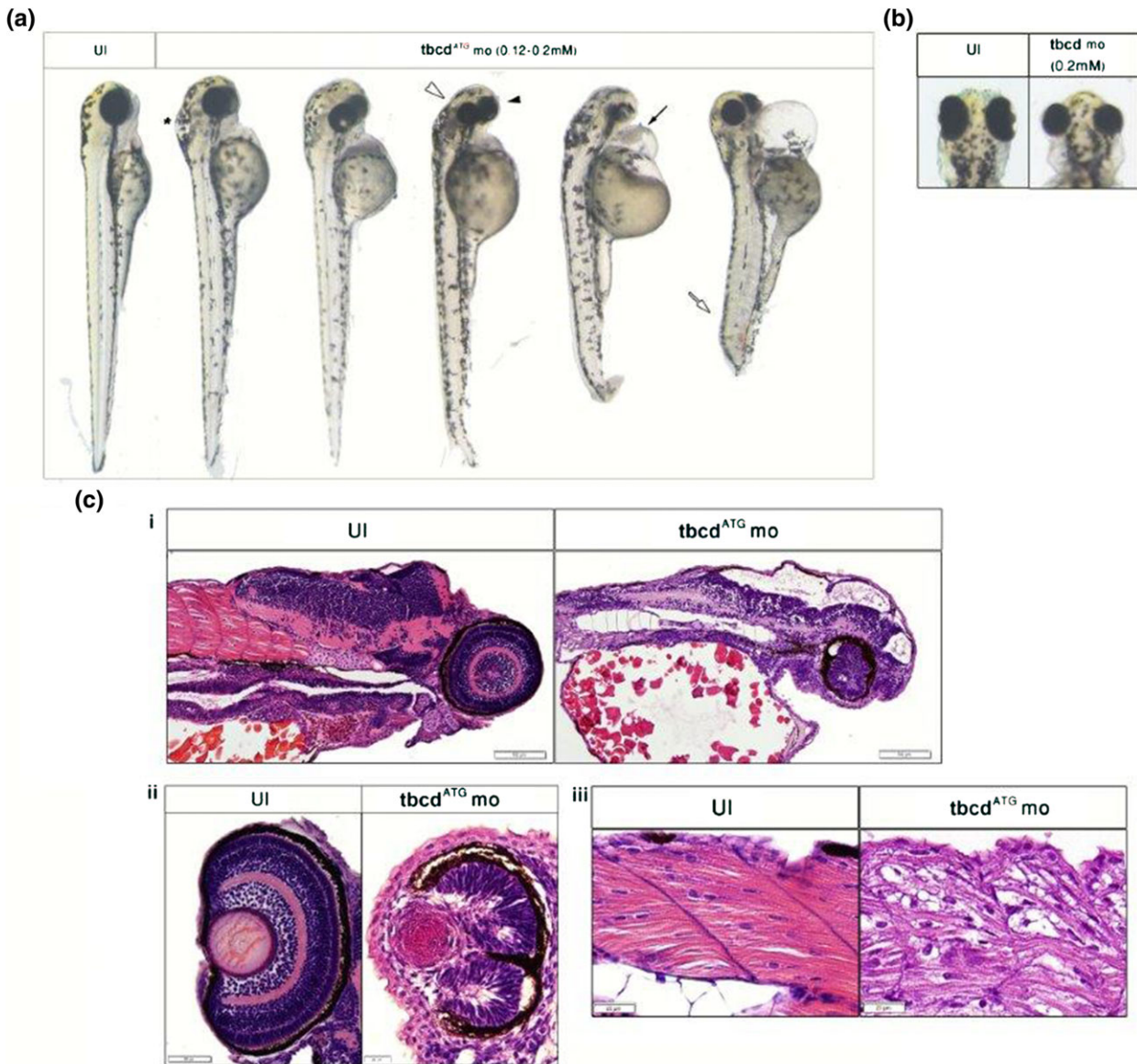


**Fig. 5.** Phenotype of morpholino (mo)-mediated tubulin cofactor D (*tbcd*) silencing in zebrafish. **(a)** *tbcd* silencing effects, from 4 days post-fertilization (4 dpf), are dose-dependent from mild to severe (left to right). The zebrafish larvae phenotype shows microcephalus (white arrowhead), scattered pigment, hydrocephalus (asterisk), small eyes (black arrowhead), heart edema (black arrow) and a short and thick tail (white arrow). **(b)** Dorsal view of *tbcd*<sup>ATG</sup> mo effects on head and eye size compared to uninjected larvae. **(c)** Histology findings for *tbcd*<sup>ATG</sup> mo-treated larvae compared to control larvae (UI, uninjected): (i) brain histology following *tbcd*<sup>ATG</sup> mo injection. *tbcd*<sup>ATG</sup> morphants display abnormally thin neural layers and decreased neural density in all brain areas, and hydrocephalus. Hematoxylin and eosin (H&E) staining, 2  $\mu$ M paraffin sections. Magnification,  $\times 20$ ; (ii) eye histology of control and *tbcd*<sup>ATG</sup> mo at 3dpf. Morphants showed smaller eye (45%) and defective lamination, while UI control larvae showed normal retinal lamination. H&E staining, 2  $\mu$ M paraffin sections. Please note that magnification of control is  $\times 40$ ; while *tbcd*<sup>ATG</sup> mo magnification is  $\times 60$ ; (iii) muscular histology following *tbcd*<sup>ATG</sup> mo injection. In the mo-treated larvae, myocytes are disorganized and the myoseptae are irregular compared with the control larvae myocytes, myotomes and myoseptae which show a regular organization. H&E staining, 2  $\mu$ M paraffin sections. Magnification,  $\times 60$ . Color figure is available in Online version.

disease-causing *TBCD* mutations perturbed TBCD levels and/or function, and showed accelerated microtubule polymerization and enhanced microtubule stability resulting from defective TBCD function. Edvardson et al. (18) reported on four individuals from two unrelated consanguineous families, showing a similar phenotype and biallelic variants in *TBCD* as well. They also showed reduced TBCD levels in cultured patient fibroblasts, and further confirmed the causative role of

the variants in *TBCD* in the disruption of the  $\alpha/\beta$ -tubulin heterodimer assembly pathway, using complementary functional assays (18). Miyake et al. (19) described eight affected patients from four unrelated families (two of whom, patients 7 and 8, corresponding to patients 2 and 3 of this report) having a similar phenotype, including postnatal microcephaly, developmental delay, seizures and diffuse brain atrophy beginning during the first year of life, found to harbor variants in *TBCD*.

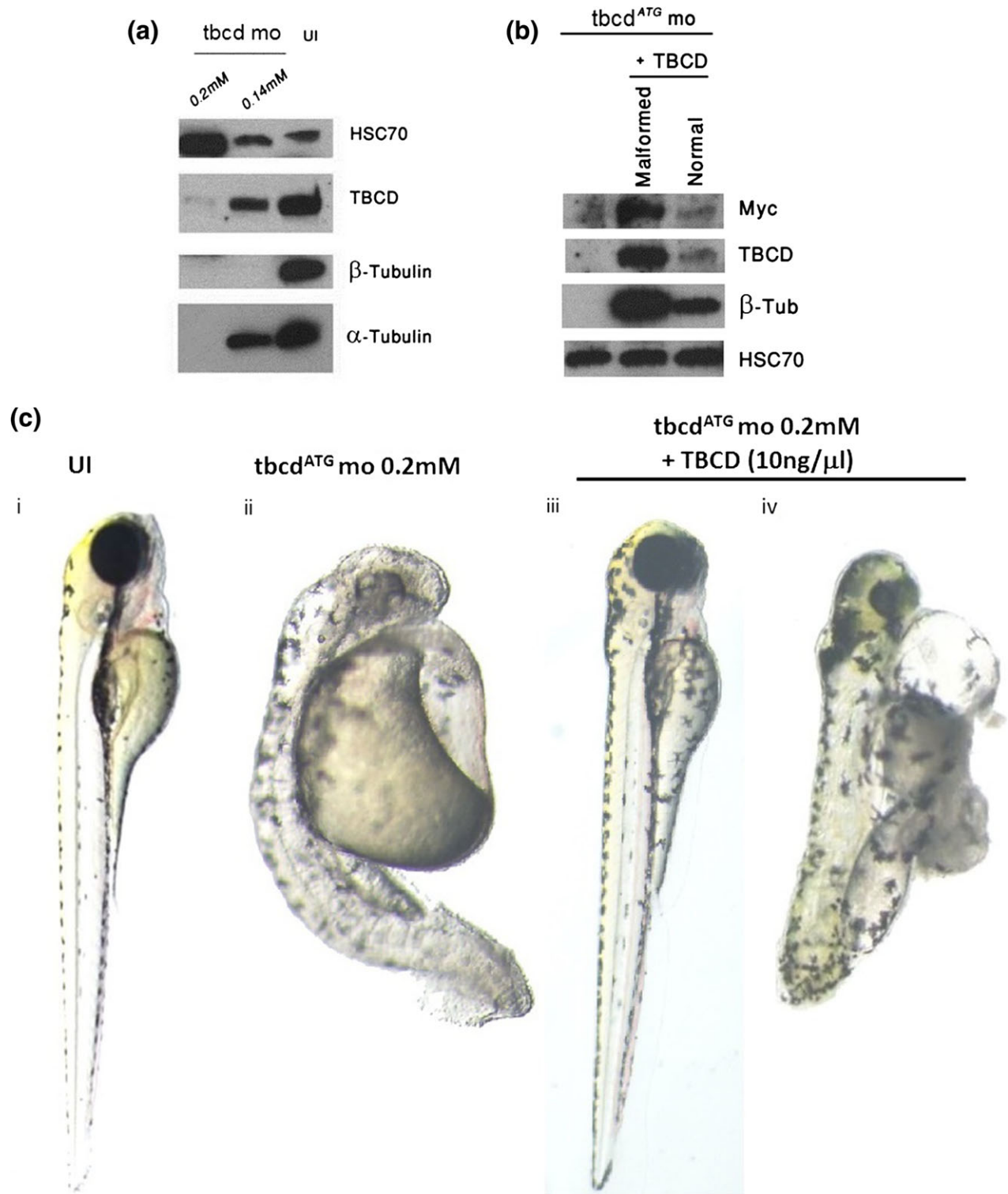


**Fig. 6.** *tbcd*/tubulin cofactor D (TBCD),  $\alpha$ -tubulin and  $\beta$ -tubulin levels, and phenotype in *tbcd*<sup>ATG</sup> mo-treated larvae with/without concomitant overexpression of TBCD. (a) *tbcd*<sup>ATG</sup> mo (0.14 and 0.2 mM) injection results in dose-dependent inhibition of *tbcd* expression and undetectable  $\beta$ -tubulin;  $\alpha$ -tubulin expression appears to depend upon the level of *tbcd* downmodulation. HSC70 levels are shown for protein load normalization. UI, uninjected. (b) Co-injection of *TBCD* in morphants. Undetectable *tbcd* and  $\beta$ -tubulin levels in *tbcd*<sup>ATG</sup> mo (0.2 mM) are rescued by co-injection with linearized *cmv::TBCD* cDNA (7 ng/ml). Exogenous myc-tagged TBCD expression is detected by using a myc-antibody. Of note, two sub-populations were apparent following co-injection: normal phenotype and severely malformed larvae. The latter showed strikingly higher expression levels of both *tbcd* and  $\beta$ -tubulin, compared to the former. (c) Severe larvae phenotype in response to TBCD overexpression at 0.2 mM. Similar to what is observed in morphants (*tbcd* mo 0.2 mM) (ii), co-injection of *cmv::TBCD* (10–20 ng/ $\mu$ l) together with *tbcd* mo resulted in either a rescued, normal-appearing larvae (iii), or a very severe phenotype (10 ng/ $\mu$ l) (iv) or high mortality (20 ng/ $\mu$ l). Uninjected embryo is shown for comparison (i). Color figure is available in Online version.

## Microcephaly, intractable seizures and developmental delay caused by biallelic variants in *TBCD*

They also provided compelling data from a brain biopsy obtained from one deceased patient, as well as demonstration of the deleterious effects of the *TBCD* variants using *Drosophila melanogaster* olfactory projection neurons (19).

Here, we report an extensive clinical characterization of five patients from three unrelated families with biallelic mutations in *TBCD*. This study provides additional data contributing to the delineation of the phenotypic spectrum resulting from biallelic *TBCD* variants. Similar to the majority of the previously reported patients, all five patients showed microcephaly, which was mostly acquired, refractory epilepsy, significant intellectual disability, and no speech (17–19). Four of five patients had severe seizures refractory to different therapies, two of them requiring vagal nerve stimulator implantation (Table 1). Interestingly, Xu et al. (29) recently studied microtubular stability presumed to be crucial for maintaining the integrity of microtubule-based axonal transport, and reported the association between microtubule dynamics and chronic epilepsy. Optic atrophy/optic disc pallor was noted in three patients, while information was not available for two. This finding was reported in six of the seven patients reported by Flex et al. (17) and in four of the eight patients reported by Miyake et al. (19) Feeding difficulties were reported in the first cohort (17) and were severe enough in two of the five patients reported here to require G-tube insertion.

Brain MRI findings, i.e. cortical atrophy with thinning of the corpus callosum and evidence of delayed myelination, were similar to the previously described cases, and noted in all four patients for which neuroimaging studies were performed. Of note, in a recent study focusing on the key neuroimaging findings of 80 patients with tubulinopathies, abnormalities of the corpus callosum were noted in 32 of 80 (40%) patients (26).

With regard to the molecular basis of disease, and consistent with the autosomal recessive pattern noted in the previously described families, the patients reported herein were either homozygous or compound heterozygotes for missense/splice site variants in *TBCD*. While patients 2 and 3 were born to consanguineous parents, the family of patient 1 did not report consanguinity. Nonetheless, his parents are of Indian-Jewish (Cochin) descent, which can be viewed as a genetic isolate (30). Indeed, the p.A475T variant identified by WES is the one reported in the previously reported affected family of Jewish-Cochin descent (18), suggesting a common ancestral mutation. Noteworthy, the maternally inherited p.A586V identified in family C who reported a mixed origin, was also identified in two siblings of Muslim-Palestinian descent (18). The two additional variants identified in our patients (p.P937R and IVS34-2A>G) were not previously described.

Similar to previous observations by Flex et al. and Edvardson et al. (17, 18), a significantly reduced amount of *TBCD* protein was documented in skin fibroblasts and lymphoblastoid lines (patient 1), confirming that defective *TBCD* represents a crucial molecular event underlying the pathogenesis of this disorder.

Microtubules frequently switch between phases of growth and shrinkage, a property known as ‘dynamic instability’ (31), which has profound impact on neuronal development and function. In addition to its role in building the core structure of microtubules, *TBCD* may modulate microtubule dynamics by promoting tubulin disassembly. Flex et al. (17) documented that defective *TBCD* function has profound effect on microtubules dynamics by perturbing the polymerization rate and stability of microtubules. By documenting an accelerated microtubule re-polymerization in primary skin fibroblasts from an affected subject, the present report confirms those observations. Similar to what was previously reported, we did not observe a significant change in the  $\alpha$ -tubulin levels in fibroblasts and lymphoblastoid cells from the same patient. However, a decrease of  $\alpha$ -tubulin expression was observed in the *tbcd*<sup>ATG</sup> morphants, a discrepancy that may be attributable to species-specific differences on the impact of aberrant *TBCD* function (24). In contrast, we documented a significant reduction in  $\beta$ -tubulin levels in *TBCD* mutated cells. The significance of this association needs to be validated and further studies are necessary to understand whether this  $\beta$ -tubulin reduction is a result of  $\beta$ -tubulin misfolding or accelerated degradation. Nonetheless, this finding suggests that dysregulation of microtubule dynamics resulting from biallelic inactivating variants in *TBCD* might result from multiple, counteracting processes controlling  $\beta$ -tubulin folding,  $\alpha/\beta$ -tubulin heterodimerization, and microtubule polymerization and de-polymerization.

Finally, we established a morpholino-mediated *tbcd* KD animal model, which presented with microcephaly, and neurodevelopmental, ophthalmologic and muscle features recapitulating the human *TBCD* variant-related phenotype. Interestingly, the morphant phenotype was evident beginning at 2 dpf, and its severity was affected by mo dosing. Histologically, brain tissue of morphants showed abnormally thin neural layers and decreased neural density when compared with control larvae, and the eyes were smaller (45%) with absent lamination. Overall, these findings further support the picture of defective *TBCD* function as the mechanism of disease of this novel tubulinopathy, and suggest impaired migration and lamination in the brain and the eyes in this KD model, which well fits with the crucial role of *TBCD* in the neuronal migration and cortical organization processes. We suggest that these dose effects reflect the crucial role of the *TBCD* in the fine tuning of the assembly and disassembly of the microtubule network which seems to be extremely sensitive to the precise *TBCD* levels. This conclusion is also consistent with those of Edvardson et al. (18) who showed that both deficiency and overexpression of *TBCD* had deleterious effects.

To conclude, the five affected individuals reported herein further delineate the newly described chaperone-related tubulinopathy, characterized by intractable epilepsy, intellectual disability and acquired microcephaly, and cortical atrophy and thinned corpus callosum as major MRI features, caused by biallelic variants in *TBCD*. The zebrafish mo model of this rare disorder recapitulates key features of the human

phenotype, underscoring the fine equilibrium of TBCD expression required for the normal function of microtubular dynamic instability. Further studies will shed additional light on the pathogenetic abnormalities that may eventually lead to therapeutic options.

### Supporting Information

Additional supporting information may be found in the online version of this article at the publisher's web-site.

### Acknowledgements

The authors wish to thank the patients and their families for their cooperation and assistance, and N. K. for his generous donation which made this study possible. This work was supported, in part, by the Italian Ministry of Health (Ricerca Corrente 2016 to E. B., M. N. and M. T.).

### References

1. Kapitein LC, Hoogenraad CC. Building the neuronal microtubule cytoskeleton. *Neuron* 2015; 87 (3): 492–506.
2. Janke C. The tubulin code: molecular components, readout mechanisms, and functions. *J Cell Biol* 2014; 206: 461–472.
3. Lewis SA, Tian G, Cowan NJ. The alpha- and beta-tubulin folding pathways. *Trends Cell Biol* 1997; 12: 479–484.
4. Tian G, Lewis SA, Feierbach B et al. Tubulin subunits exist in an activated conformational state generated and maintained by protein cofactors. *J Cell Biol* 1997; 138: 821–832.
5. López-Fanarraga M, Avila J, Guasch A et al. Review: postchaperone tubulin folding cofactors and their role in microtubule dynamics. *J Struct Biol* 2001; 135: 219–229.
6. Szymanski D. Tubulin folding cofactors: half a dozen for a dimer. *Curr Biol* 2002; 12 (22): R767–R769.
7. Zhou C, Chunningham L, Marcus AI, Li Y, Kahn RA. Arl2 and Arl3 regulate different microtubule-dependent processes. *Mol Biol Cell* 2006; 17: 2476–2487.
8. Parvari R, Hershkovitz E, Grossman N et al. Mutation of TBCE causes hypoparathyroidism-retardation-dysmorphism and autosomal recessive Kenny-Caffey syndrome. *Nat Genet* 2002; 32: 448–452.
9. Keays DA, Tian G, Poirier K et al. Mutations in alpha-tubulin cause abnormal neuronal migration in mice and lissencephaly in humans. *Cell* 2007; 128: 45–57.
10. Jaglin XH, Poirier K, Saillour Y et al. Mutations in the beta-tubulin gene TUBB2B result in asymmetrical polymicrogyria. *Nat Genet* 2009; 41: 746–752.
11. Tischfield MA, Cederquist GY, Gupta ML Jr, Engle EC. Phenotypic spectrum of the tubulin-related disorders and functional implications of disease-causing mutations. *Curr Opin Genet Dev* 2011; 21: 286–294.
12. Breus M, Keays DA. Microtubules and neurodevelopmental disease: the movers and the makers. *Adv Exp Med Biol* 2014; 800: 75–96.

13. Simons C, Wolf NI, McNeil N et al. A de novo mutation in the  $\beta$ -tubulin gene TUBB4A results in the leukoencephalopathy hypomyelination with atrophy of the basal ganglia and cerebellum. *Am J Hum Genet* 2013; 92 (5): 767–773.
14. Smith BN, Ticozzi N, Fallini C et al. Exome-wide rare variant analysis identifies TUBA4A mutations associated with familial ALS. *Neuron* 2014; 84 (2): 324–331.
15. Dubey J, Ratnakaran N, Koushika SP. Neurodegeneration and microtubule dynamics: death by a thousand cuts. *Front Cell Neurosci* 2015; 9: 343.
16. Sferra A, Baillat G, Rizza T et al. *TBCE* mutations cause early-onset progressive encephalopathy with distal spinal muscular atrophy. *Am J Hum Genet* 2016; 99 (4): 974–983.
17. Flex E, Niceta M, Cecchetti S et al. Biallelic mutations in *TBCD*, encoding the tubulin folding cofactor D, perturb microtubule dynamics and cause early-onset encephalopathy. *Am J Hum Genet* 2016; 99 (4): 962–973.
18. Edvardson S, Tian G, Cullen H et al. Infantile neurodegenerative disorder associated with mutations in *TBCD*, an essential gene in the tubulin heterodimer assembly pathway. *Hum Mol Genet* 2016. Epub ahead of print.
19. Miyake N, Fukai R, Ohba C et al. Biallelic *TBCD* mutations cause early-onset neurodegenerative encephalopathy. *Am J Hum Genet* 2016; 99 (4): 950–961.
20. Tian G, Huang Y, Rommelaere H, Vandekerckhove J, Ampe C, Cowan NJ. Pathway leading to correctly folded beta-tubulin. *Cell* 1996; 86 (2): 287–296.
21. Martín L, Fanarraga ML, Aloria K, Zabala JC. Tubulin folding cofactor D is a microtubule destabilizing protein. *FEBS Lett* 2000; 470 (1): 93–95.
22. Fanarraga ML, Bellido J, Jaén C, Villegas JC, Zabala JC. TBCD links centriologensis, spindle microtubule dynamics, and midbody abscission in human cells. *PLoS One* 2010; 5 (1): e8846.
23. Cunningham LA, Kahn RA. Cofactor D functions as a centrosomal protein and is required for the recruitment of the gamma-tubulin ring complex at centrosomes and organization of the mitotic spindle. *J Biol Chem* 2008; 283 (11): 7155–7165.
24. Tian G, Thomas S, Cowan NJ. Effect of TBCD and its regulatory interactor Arl2 on tubulin and microtubule integrity. *Cytoskeleton (Hoboken)* 2010; 67 (11): 706–714.
25. Okumura M, Sakuma C, Miura M, Chihara T. Linking cell surface receptors to microtubules: tubulin folding cofactor D mediates Dscam functions during neuronal morphogenesis. *J Neurosci* 2015; 35 (5): 1979–1990.
26. Bahi-Buisson N, Poirier K, Fourniol F et al. The wide spectrum of tubulinopathies: what are the key features for the diagnosis? *Brain* 2014; 137 (Pt 6): 1676–1700.
27. Sakuma C, Okumura M, Umehara T, Miura M, Chihara T. A STRIPAK component strip regulates neuronal morphogenesis by affecting microtubule stability. *Sci Rep* 2015; 5: 17769.
28. Poulton CJ, Schot R, Seufert K et al. Severe presentation of WDR62 mutation: is there a role for modifying genetic factors? *Am J Med Genet A* 2014; 164A (9): 2161–2171.
29. Xu X, Hu Y, Xiong Y et al. Association of microtubule dynamics with chronic epilepsy. *Mol Neurobiol* 2016; 53 (7): 5013–5024.
30. Waldman YY, Biddanda A, Dubrovsky M, et al. The genetic history of Cochlin Jews from India. *Hum Genet* 2016; 135 (10): 27–43.
31. Brouhard GJ. Dynamic instability 30 years later: complexities in microtubule growth and catastrophe. *Mol Biol Cell* 2015; 26 (7): 1207–1210.